BEAM OBSERVATIONS WITH ELECTRON CLOUD IN THE CERN PS & SPS COMPLEX

G. Arduini, T. Bohl, K. Cornelis, W. Höfle, E. Métral, F. Zimmermann, AB Department, CERN, Geneva, Switzerland

Abstract

With the start of the machine studies to characterize the behaviour of the LHC beam in the SPS in 1999, it became evident that electron multipacting was occurring in the SPS vacuum chambers in the presence of this beam. Multipacting induces dramatic pressure increases preventing stable operation, it limits the performance of beam instrumentation and high voltage electrostatic devices (e.g. electrostatic septa) and it induces strong transverse instabilities leading to emittance dilution. Although an increase of the threshold bunch population for multipacting can be obtained by beam conditioning ("scrubbing"), multipacting persists in the arcs for the nominal LHC bunch population and electron cloud instabilities remain an issue for the LHC beam.

A programme of studies has been launched since 1999 to study the electron cloud build-up and related instabilities in the SPS and in the PS for the LHC and fixed target beams. The experimental tools and analysis developed so far are presented together with the results of the observations. The countermeasures applied in the PS Complex & SPS against the electron cloud instability are also briefly discussed.

INTRODUCTION

The main beam parameters for the LHC and fixed target beams are listed in Tables 1 and 2.

Table 1: The LHC beam in CERN PS and SPS [1]

	PS@extr.	SPS@inj.	SPS@extr
Momentum [GeV/c]	26	26	450
Revolution period [μs]	2.1	23.07	23.05
Tunes (H/V)	6.25	26.185/26.13	
Gamma transition	6.1	22.8	
Max. n. of batches	1	4	
n. bunches/batch	72	72	
Nominal N_b [10^{11}]	1.15	1.15	
Bunch spacing [ns]	24.97	24.97	24.95
Full bunch length [ns]	4-16*	4	<2
Batch spacing [ns]	-	224.7	224.6
r.m.s. $\varepsilon^*_{H,V}$ [μm]	3	3	3.5
ε_L [eV s]	0.35	0.35	<0.8

* The bunch length is reduced from 16 to 4 ns by a non-adiabatic bunch compression prior to extraction. This process takes approximately 100 turns (~200 μs)

Table 2: The Fixed Target beam in CERN SPS

	SPS@inj.	SPS@extr
Momentum [GeV/c]	14	400
Revolution period [μs]	23.11	23.05
Tunes (H/V)	26.62/26.58	
Gamma transition	23.2	
Max. n. of batches	2	
n. bunches/batch	2100	
Nominal N_b [10^{11}]	0.1 – 0.2	
Bunch spacing [ns]	5.00	4.99
Full bunch length [ns]	4	<3
Batch spacing [ns]	1050	1048
r.m.s. $\varepsilon^*_{H,V}$ [μm]	<10,<7.5	<12,<12
ε_L [eV s]	0.2	0.6 - 2

ELECTRON MULTIPACTING INDUCED BY THE LHC BEAM

Because of the high bunch population (N_b) and the 25-ns bunch spacing the LHC beam induces electron multipacting in the SPS for N_b higher than a given threshold bunch population (N_{th}) depending on the Secondary Emission Yield (SEY) of the surface of the vacuum chamber and on the presence of a magnetic field. In the stainless steel vacuum chamber of the bending magnets, covering 70% of the SPS circumference, N_{th}~0.2-0.3×10^{11} while in the straight sections (field-free regions) N_{th}~0.6×10^{11} (for 1 batch at 26 GeV/c). After a period of conditioning with LHC beam at the beginning of the 2002 run [2] the threshold was increased to about N_{th}~0.8×10^{11} in the arcs (still lower than the nominal bunch population) and to N_{th}~1.1×10^{11} in the straight sections.

Above the multipacting threshold the following phenomena are observed:

- Dramatic dynamic pressure increases (by more than a factor 100) mainly in the arcs [2][3] (see Fig.1) leading to residual pressures close to the beam abort level (~10^{-6} - 10^{-5} mbar).
- Distortion of the baseline of the signal provided by the electrostatic pick-ups used for the transverse feedback (Fig. 2) for $N_b > N_{th}$ [4] preventing the reliable operation of the system. Such effect could be suppressed by applying a solenoidal field of approximately 100 G.

- High noise in the Secondary Emission Monitors used for the measurements of the transverse emittance in the transfer line from PS to SPS. This occurs only when the non-adiabatic bunch compression for the nominal LHC beam is applied (Fig. 3). As a consequence, beam profiles for the nominal LHC beam can be measured only with Optical Transition Radiation detectors.

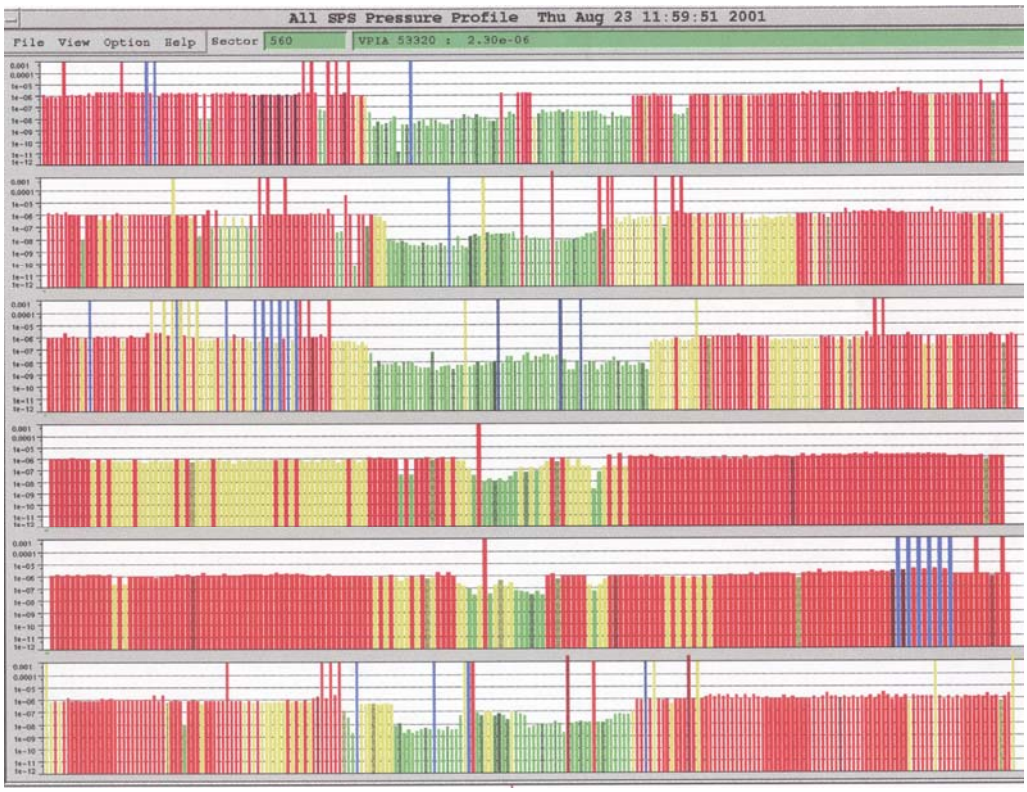

Figure 1. Residual pressure P in the SPS sextants in the presence of the nominal LHC beam. The colour code is the following: red = $P > 10^{-6}$ mbar, yellow = $10^{-7} < P < 10^{-6}$ mbar, green = $P < 10^{-7}$ mbar. The straight sections are located in the centre of each of the six graphs. It must be noted that the gauges are not distributed uniformly in the ring. The long straight sections 1 (top), 2, 3 and 6 (bottom) are more densely instrumented because of the presence of the injection (straight section 1) and extraction (straight sections 2 and 6) elements and of the RF accelerating cavities (straight section 3).

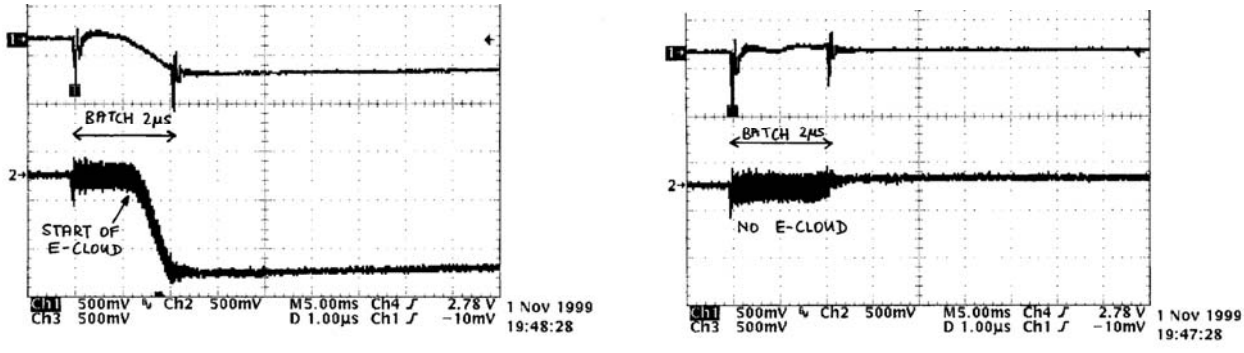

Figure 2. Horizontal (top) and vertical (bottom) signals provided by the SPS transverse feedback pick-up without solenoidal field (left) and with a solenoidal field of 100 G (right), in the presence of LHC beam with $N_b = 0.5\times10^{11} > N_{th} \sim 0.2\text{-}0.3\times10^{11}$.

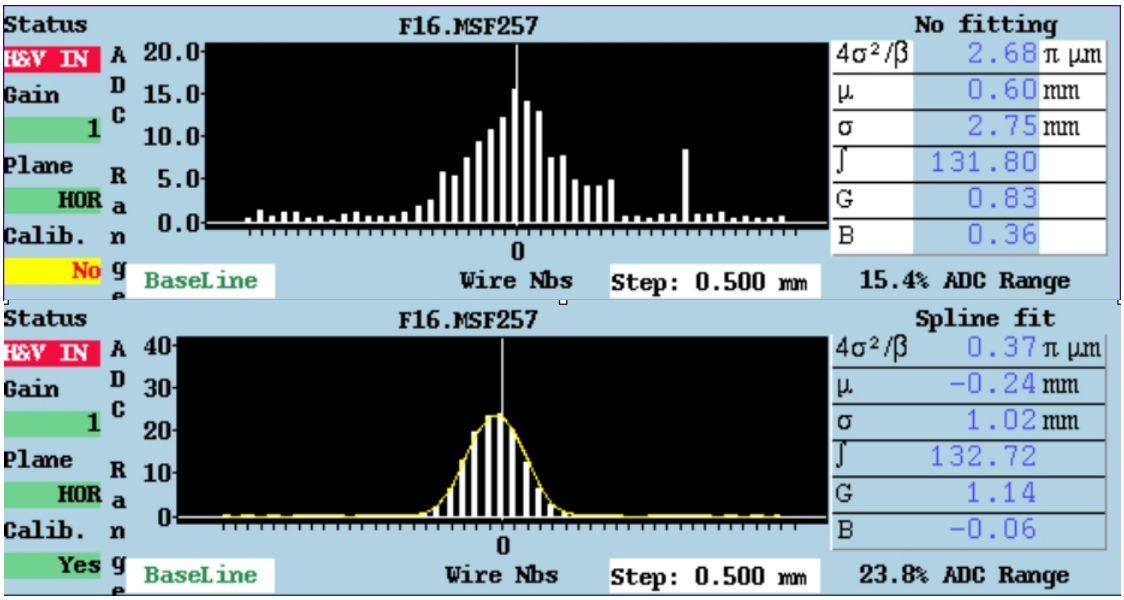

Figure 3. Transverse beam profile from a Secondary Emission Monitor in the PS to SPS transfer line vs. bunch length. Top: nominal LHC beam with bunch rotation (full bunch length = 4 ns). Bottom: LHC beam without bunch rotation (full bunch length = 16 ns).

All the above observations are consistent with electron cloud build-up to densities of 10^{11}-10^{12} e^-/m^3 along the LHC bunch train. The original seed electrons are produced by ionisation of the residual gas (~10^8 e^-/m^3/turn for an LHC bunch train, for a residual vacuum pressure of 10^{-8} mbar and an ionisation cross-section of a few Mbarn). Multipacting occurs in a single turn as observed in the PS to SPS transfer line.

EFFECTS ON THE LHC BEAM IN THE SPS

Above the multipacting threshold horizontal and vertical emittance growth affecting mainly the tail of the batch occurs at injection (Fig. 4) when the LHC beam is injected in a machine with low positive chromaticity ($\xi = (\Delta Q/Q)/(\Delta p/p) \sim 0.02$-$0.05$), coupling corrected (Closest Tune Approach ~ 0.001) and detuning with amplitude compensated by means of machine octupoles. This is observed even when the transverse feedback is active. The blow-up of the tail of the batch is such that the physical aperture of the machine is hit in the vertical plane and fast losses are observed a few ms after injection mainly affecting the tail of the bunch train (Fig. 5).

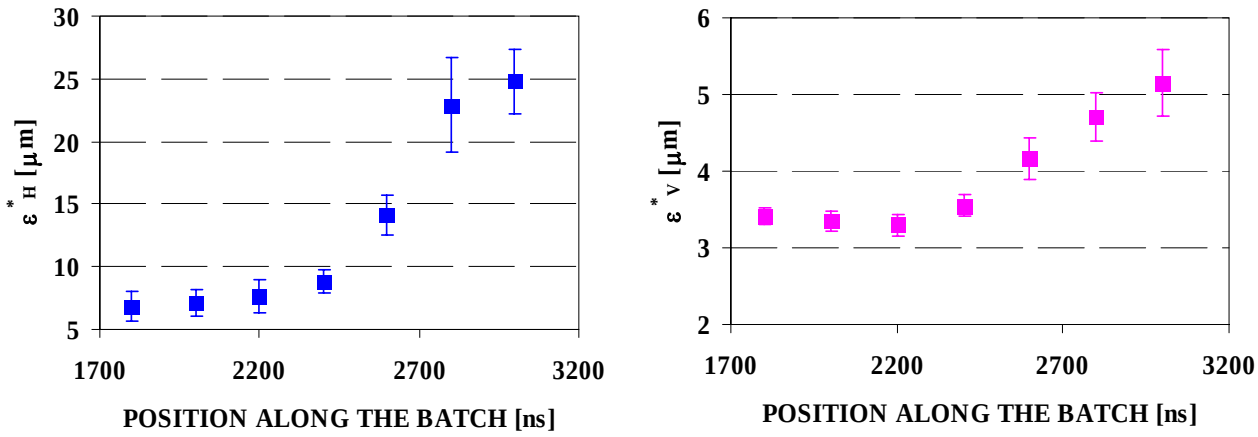

Figure 4. Rms horizontal (left) and vertical (right) normalised emittances along the LHC batch (first 48 bunches) few tens of ms after injection. $N_b = 0.8\times10^{11} > N_{th} \sim 0.2$-$0.3\times10^{11}$.

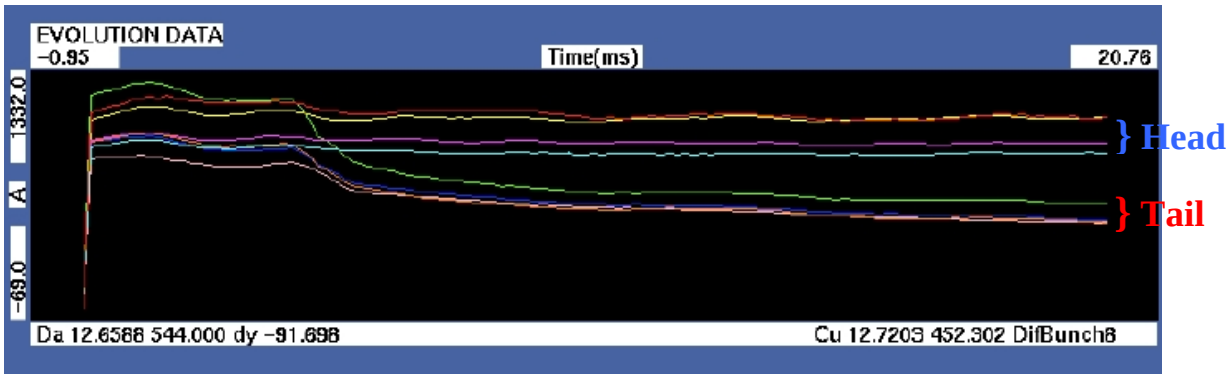

Figure 5. Relative bunch intensity evolution for the LHC beam over 20 ms. Losses are affecting the trailing bunches only. $N_b = 0.8\times10^{11} > N_{th} \sim 0.2\text{-}0.3\times10^{11}$.

ELECTRON CLOUD INSTABILITY IN THE SPS WITH LHC BEAM - OBSERVATIONS

The measured emittance dilution and beam losses are the result of an Electron Cloud Instability (ECI) developing from the tail and progressing to the head of the batch for $N_b > N_{th}$. For a single batch with nominal bunch population all bunches except the first 10-15 are affected. The characteristics of the instability are significantly different in the horizontal and vertical planes in the SPS. This different behaviour is well illustrated in Fig. 6 [5] representing a snapshot of the horizontal and vertical position of the first 48 bunches in the batch. The signal is provided by a wide-band strip-line coupler 60 cm long [6] with a sampling time of 0.5 ns permitting to resolve transverse motion inside individual bunches. Visible are also reflections occurring with a delay of 4 ns resulting from the finite length of the monitor. In both planes the instability starts after about 16 bunches.

In the horizontal plane a slow wave over more than 20 bunches is visible, while in the vertical plane no evident phase correlation can be distinguished between subsequent bunches. The Electron Cloud Instability is:

- a coupled-bunch instability in the horizontal plane,
- a single-bunch instability in the vertical plane.

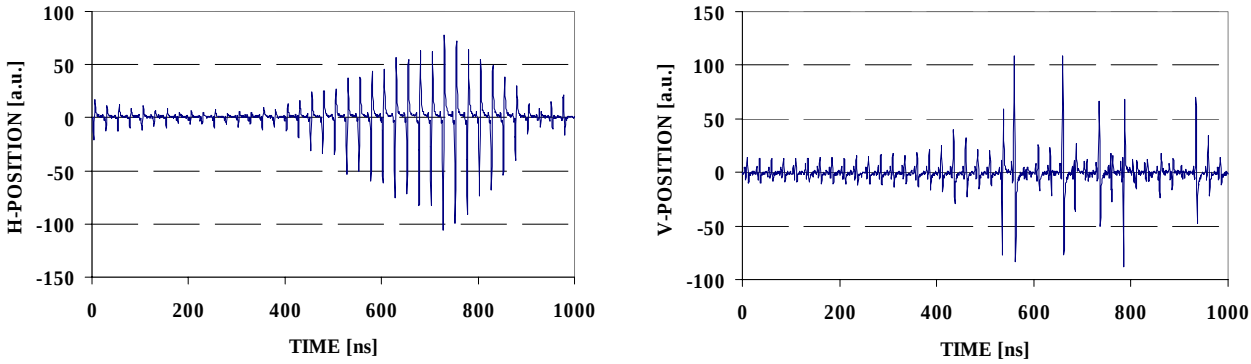

Figure 6. Snapshot of the horizontal (left) and vertical (right) position of the first 48 bunches of the LHC bunch train. $N_b = 0.8\times10^{11} > N_{th} \sim 0.2\text{-}0.3\times10^{11}$.

Horizontal Instability

Because of its nature, the coupled-bunch instability occurring in the horizontal plane has been studied mainly by measuring the motion of the centroid of the individual bunches of the LHC beam. Fig. 7a shows the amplitude of the oscillation of the 72 bunches of the LHC beam ($N_b = 0.3\times10^{11} > N_{th} \sim 0.2\text{-}0.3\times10^{11}$) recorded over 1000 turns (~23 ms). Injection occurs at turn number 71. Only the tail of the batch is affected significantly and the growth time is about 40 turns. The tune spectrum along the batch is also shown in Fig. 7b: besides the unperturbed coherent tune line (~0.627) a second line is appearing starting from bunch 16 and it is growing in amplitude and separating from the main tune line. At the tail of the batch (after bunch 50), where the electron cloud density saturates, the separation is about 0.025. Fig 7c shows a 2-dimensional Fourier transform of the data. The mode number is the number of wavelengths of the oscillation in one machine turn. The distance between two consecutive LHC bunches

is 25 ns i.e. 1/924 of a machine turn therefore the maximum mode number than can be resolved is 462. Only low frequency modes (few MHz, i.e. modes with wavelength larger than 1/100 of the machine circumference) are visible for both the observed tune lines. The line at higher tune shows slightly higher frequency modes as compared to the unperturbed tune line.

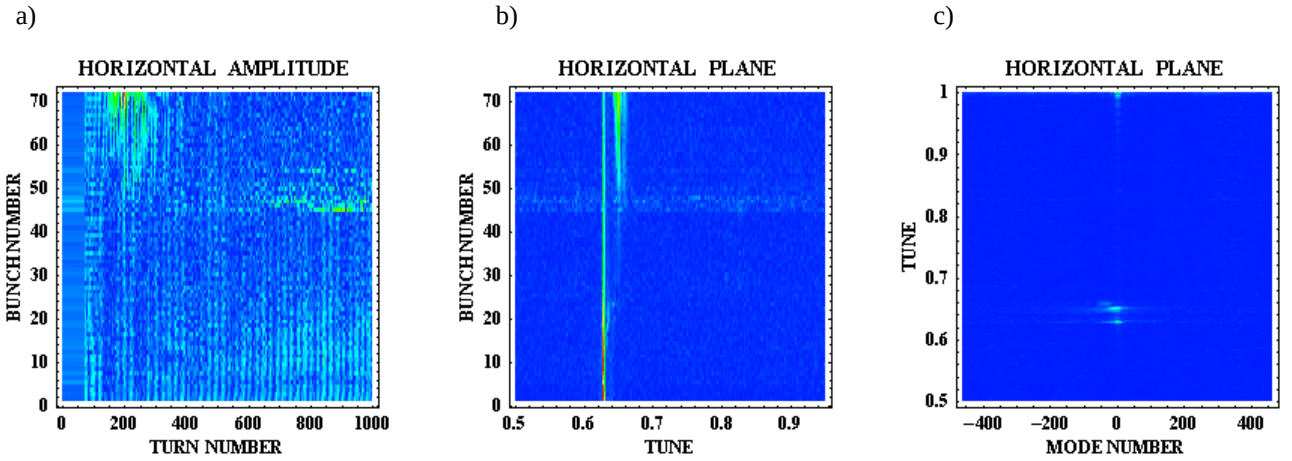

Figure 7. Density plots of the oscillation amplitude vs. turn and bunch number (a), tune spectrum vs. bunch number (b), tune and mode number spectra (c) in the horizontal plane. $N_b = 0.3\times10^{11} > N_{th} \sim 0.2\text{-}0.3\times10^{11}$. Injection occurs at turn 71 from the start of the acquisition. In the plots blue points correspond to low amplitudes and red ones to high amplitudes.

The same data can be analysed in time-domain by applying Singular Value Decomposition to study the coupled-bunch instability [7]. Let **X** be the matrix (1000 × 72) whose elements $x_{t,b} = x(t,b)$ (t=1,…,1000 and b=1,…,72) are the positions of bunch number b at turn t, then **X** can be decomposed in the product

$$\mathbf{X} = \mathbf{U}^{\mathbf{T}}\mathbf{W}\mathbf{V}$$

where **U** (72 × 1000) is a matrix with orthonormal rows, **V** (72 × 72) is an orthogonal matrix and **W** (72 × 72) is a diagonal matrix, therefore

$$x(t,b) = \sum_{k=1}^{72} \lambda_k u_k(t) v_k(b) \quad \text{with}$$

$$\lambda_k = W_{k,k},\ u_k(t) = U_{k,t},\ v_k(b) = V_{k,b}$$

$$\sum_{t=1}^{1000} u_k(t) u_l(t) = \delta_{kl} \quad \text{and} \quad \sum_{b=1}^{72} v_k(b) v_l(b) = \delta_{kl}$$

for each k,l (1,…,72). $u_k(t)$ and $v_k(b)$ represent a time and spatial pattern (improperly called "modes" in the following) of the beam oscillation, respectively. The weight of the contribution of each pattern to the oscillation is determined by λ_k.

Figure 8 shows the result of such analysis for N_b=0.3×10^{11}. The spatial structure evidences only low order coupled-bunch modes. The first "mode" (Fig. 8a) is almost a rigid oscillation of the whole bunch train (note the scale) and its oscillation frequency corresponds to the unperturbed fractional tune (0.627). The second "mode" (Fig. 8b), affecting mainly the tail of the batch after bunch 50, oscillates at a tune of 0.65. It is interesting to note a "knee" in the spatial pattern at about bunch 50 (Fig. 8b) where also the oscillations start to have significant amplitude and where the electron cloud saturates.

Fig. 9 represents the beam centroid position data in normalised phase space coordinates (both Cartesian and Polar representations) for the first and the 50th bunch in the train. The tilt in the phase space distribution particularly evident for bunch 50 could be an indication of the presence of an additional quadrupolar field, due to the electron cloud.

Figure 10 shows the dependence of the tune on the amplitude of oscillation for bunch 50. The amplitude of the oscillation is expressed in arbitrary units because the beam position monitor used for the measurement was not calibrated. The tune is calculated as a sliding average on the phase advance per turn over 32 turns. The phase advance and the amplitude are calculated from the positions of the beam at two consecutive turns and from the known 1-turn transfer matrix of the SPS machine. No significant detuning with amplitude is visible.

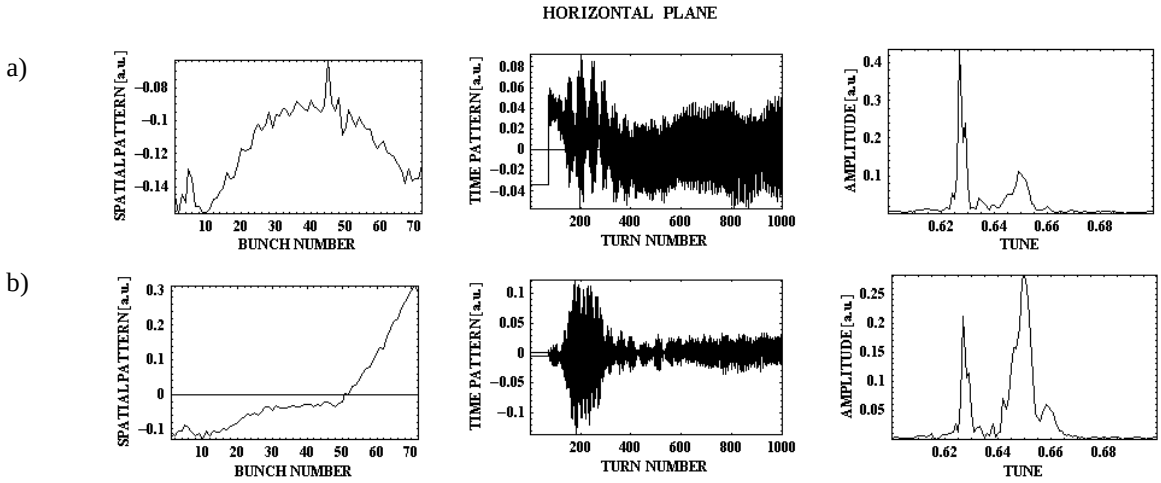

Figure 8. Time-domain analysis of the data corresponding to Fig. 7. N_b=0.3×10^{11} > N_{th}~0.2-0.3×10^{11}. The two most important (i.e. with larger λ_k) spatial and temporal patterns together with the Fourier transform of the temporal pattern are shown.

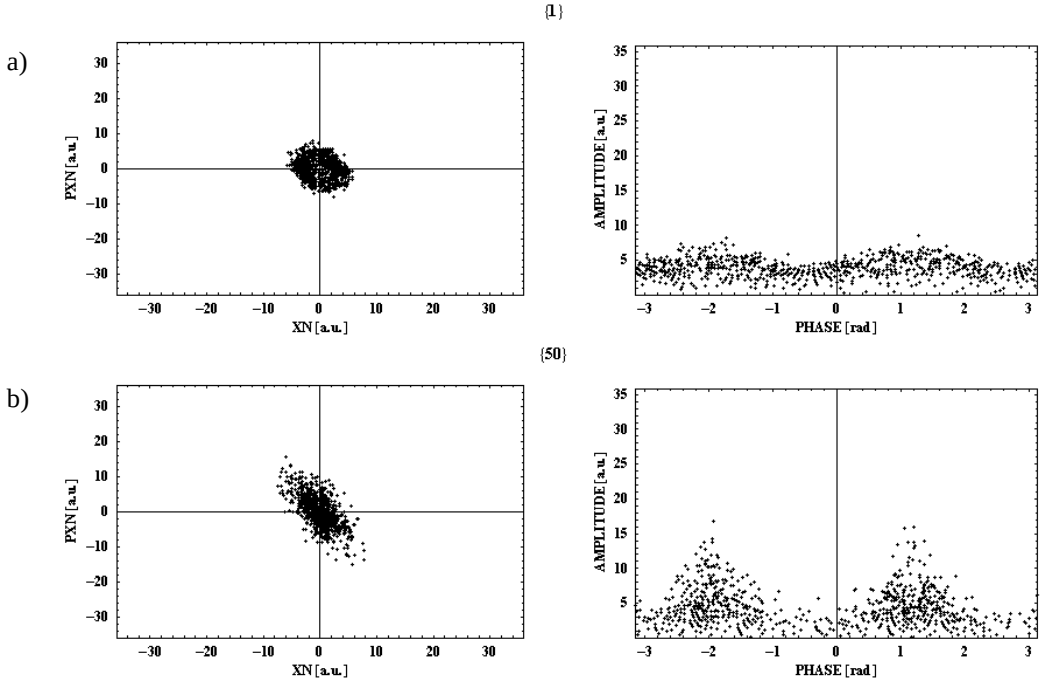

Figure 9. Phase-space reconstruction of the oscillation of bunch number 1 (a) and 50 (b) in normalised coordinates (Cartesian plots in the left column and Polar plots in the right column). N_b= 0.3×10^{11} > N_{th} ~ 0.2-0.3×10^{11}.

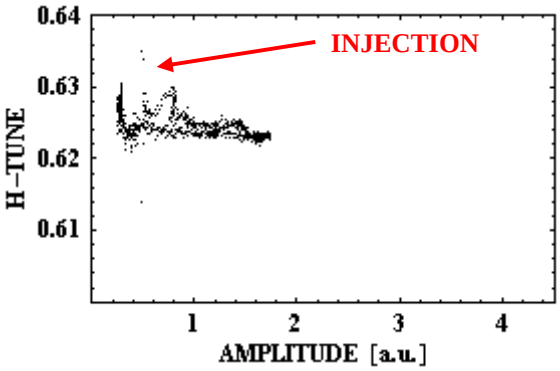

Figure 10. Tune vs. amplitude of oscillation for bunch number 50. N_b= 0.3×10^{11} > N_{th} ~ 0.2-0.3×10^{11}.

Similar measurements have been performed for N_b=0.5×10^{11} > N_{th} ~ 0.2-0.3×10^{11} with the same machine settings. The results of the measurements are presented in Figs. 11 and 12. Injection occurs at turn 30 from the start of the acquisition. Also in this case the instability develops starting from the tail of the batch and it then propagates to the head of the batch. The rise time of the instability is larger than 40 turns (hence slower than at N_b=0.3×10^{11}).

The tune variation through the batch is much less marked than for the lower intensity and for bunches near bunch 15 is negative (Fig. 11 b). The modes with higher mode number have slightly lower tune (Fig, 11 c).

The negative detuning is particularly important at large amplitudes. An important hysteresis effect is also visible. This is an indication of a pronounced non linear dependence of the electron-cloud coupling strength among bunches (Fig. 12). It must be noted that for a beam with nominal emittance at injection an oscillation with amplitude 10^{-3} $m^{1/2}$ corresponds to 3 beam sigmas (this is no longer valid in case of an important blow-up).

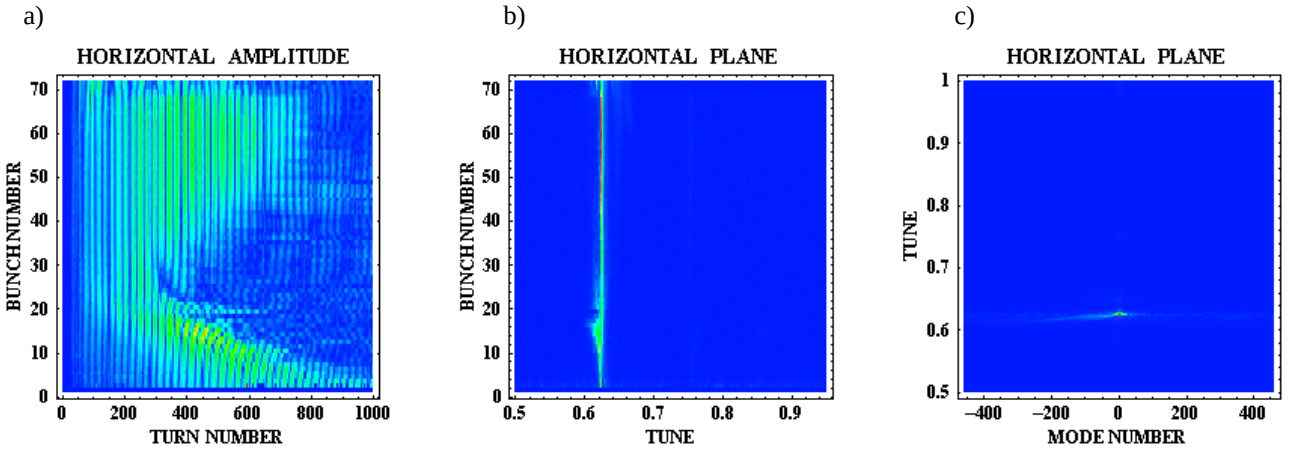

Figure 11.Density plots of the oscillation amplitude vs. turn and bunch number (a), tune spectrum vs. bunch number (b), tune and mode number spectra (c) in the horizontal plane. N_b= 0.5×10^{11} > N_{th} ~ 0.2-0.3×10^{11}. Injection occurs at turn 30 from the start of the acquisition.

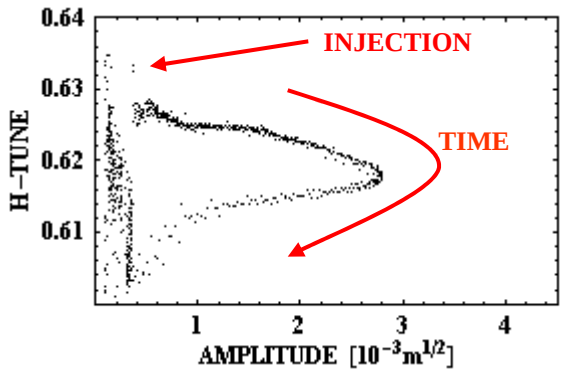

Figure 12. Tune vs. amplitude of oscillation for bunch number 15. N_b= 0.5×10^{11} > N_{th}=0.2-0.3×10^{11}.

Figures 13 and 14 present the results of the measurements performed with N_b~1.1×10^{11}p > N_{th}~0.8×10^{11} (after scrubbing). In this case a different working point (q_H=0.185, q_V=0.13 – the LHC beam working point for high intensity) has been used. Again the instability develops from the tail to the head of the batch and the measured growth rate is 40 turns.

The measured detuning with amplitude for the "transition bunches" shows a significant positive detuning for low amplitudes (+0.01 in about 1 beam sigma for nominal beam emittance) followed by a negative detuning. Hysteresis phenomena are visible. These are the consequence of the inhomogeneous distribution of the electron cloud around the beam.

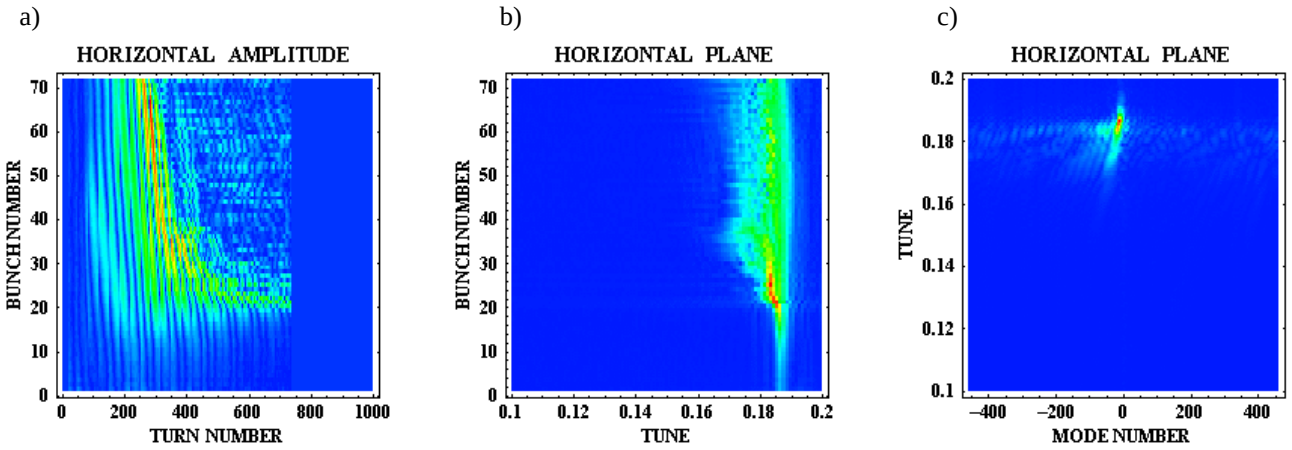

Figure 13. Density plots of the oscillation amplitude vs. turn and bunch number (a), tune spectrum vs. bunch number (b), tune and mode number spectra (c) in the horizontal plane. N_b= 1.1×10^{11} > N_{th} ~ 0.8×10^{11}. Injection occurs at turn 21 from the start of the acquisition which covers 738 turns.

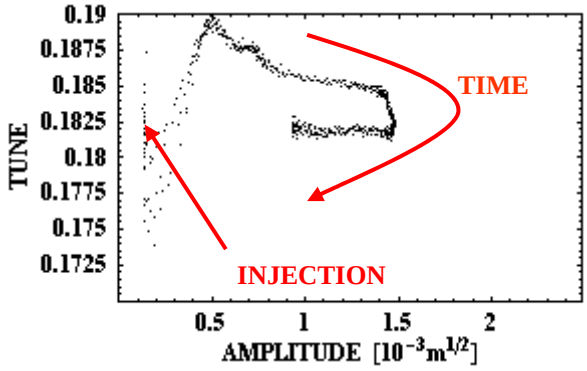

Figure 14. Tune vs. amplitude of oscillation for bunch number 25. N_b= 1.1×10^{11} > N_{th} ~ 0.8×10^{11}.

Vertical Instability

In the vertical plane the electron cloud instability looks like a single-bunch instability. Figure 15 shows the results of the bunch centroid measurements for N_b=0.3×10^{11}. The mode spectrum extends over the whole frequency range like a white spectrum and it is compatible with uncorrelated single-bunch dipolar (or higher order) oscillations at frequency $(n+q_V)f_{rev}$. The instability mainly affects the tail of the batch and the rise time is decreasing with the bunch population (the maximum amplitude of oscillation is achieved in ~600 turns for N_b=0.3×10^{11} and in 300 turns for N_b=0.5×10^{11}).

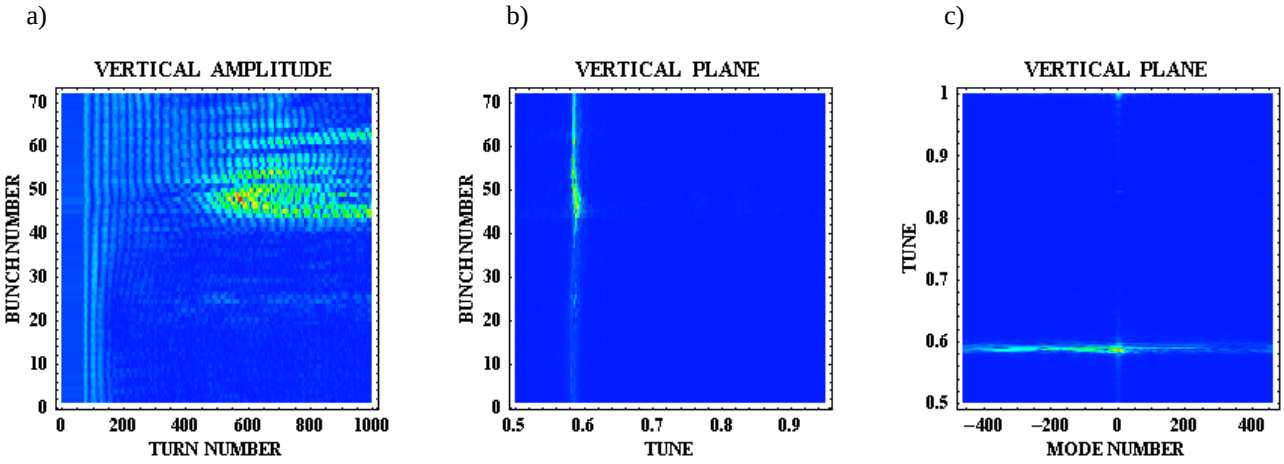

Figure 15.Density plots of the oscillation amplitude vs. turn and bunch number (a), tune spectrum vs. bunch number (b), tune and mode number spectra (c) in the vertical plane. N_b= 0.3×10^{11} > N_{th} ~ 0.2-0.3×10^{11}. Injection occurs at turn 71 from the start of the acquisition.

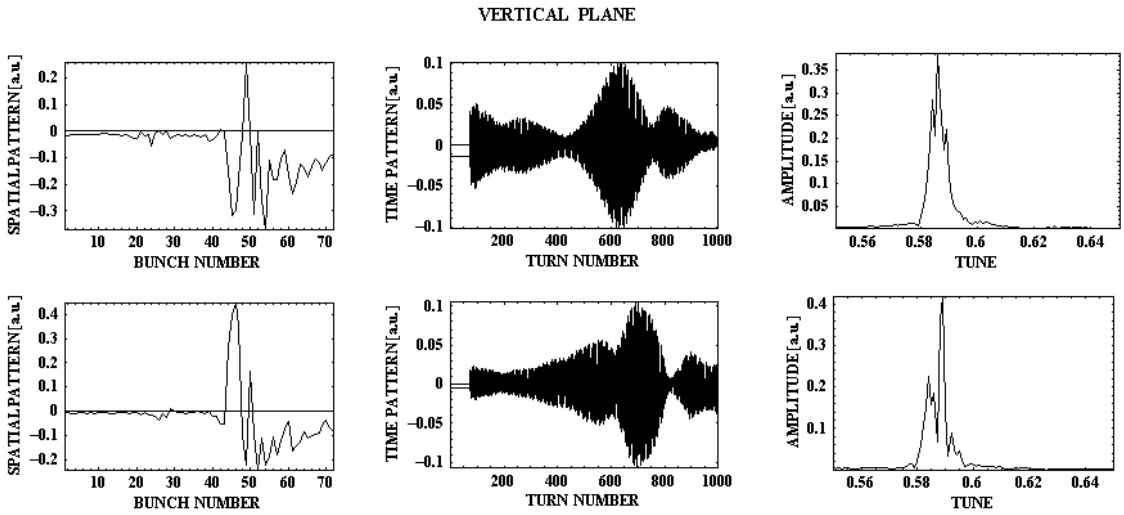

Figure 16. Time-domain analysis of the data corresponding to Fig. 15. N_b= 0.3×10^{11} > N_{th} ~ 0.2-0.3×10^{11}. The two most important (i.e. with larger λ_k) spatial and temporal patterns together with the Fourier transform of the temporal pattern are shown.

The time-domain analysis (spatial pattern in Fig. 16) of the data confirms the higher frequency nature of the vertical instability: modes close to 20 MHz are visible in the tail of the batch. Sidebands (with separation close to

the synchrotron tune Q_s~0.004) are also observed and they could be an indication of the head-tail nature of the oscillation.

Figure 17 shows the Fourier spectra of the sum and delta signals provided by a wide-band strip-line monitor for different bunches of the LHC bunch train. The comparison of the spectra for the sum and delta signals reveals some activity around 700 MHz for the trailing bunches (after bunch 15). It must be noted that the strip-line coupler, because of its length (~60 cm), has a transfer functions with zeroes at frequencies which are multiples of ~250 MHz.

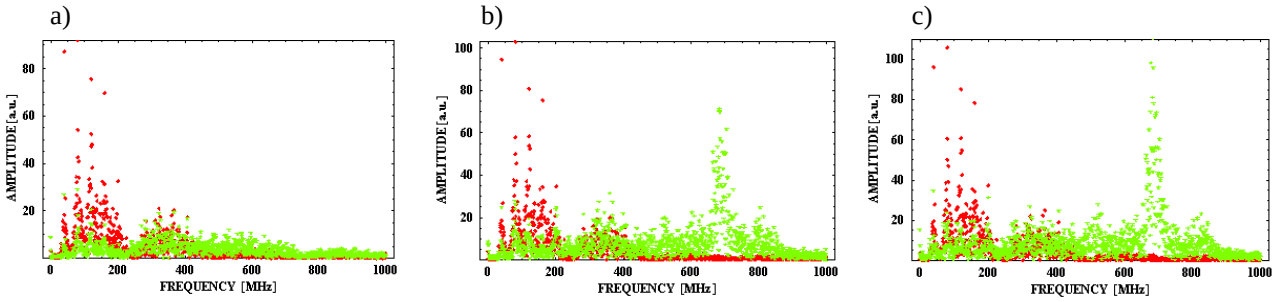

Figure 17. Fourier spectra of the sum (red) and delta (green) signals from a wideband vertical pick-up for the leading (a) bunch of the LHC bunch train and for bunch number 15 (b) and 39 (c). N_b= 0.8×10^{11} > N_{th}=0.2-0.3×10^{11}.

ELECTRON CLOUD INSTABILITY IN THE SPS WITH LHC BEAM – QUALITATIVE MODEL

The characteristics of the Electron Cloud Instability in the SPS with LHC beam are a consequence of the transverse properties of the electron cloud in the arcs. The main bending magnets are installed over 70 % of the SPS circumference and N_{th} is lower in dipole field regions than in field-free sections [3].

Horizontal plane

In a dipole field electrons are bouncing up and down in the vacuum chamber and are tightly bound to the magnetic field lines around which they spiral. Due to the presence of the magnetic field no net horizontal motion is imparted to the electrons by a bunch during its passage. Therefore no significant pinch of the electron cloud occurs in the horizontal plane during the bunch passage and the electron cloud can only couple subsequent bunches. For that reason only coupled-bunch instabilities are detected in the horizontal plane.

The dependence of the SEY on the electron energy and the dependence of the energy gain of the electrons on their horizontal offset with respect to the beam centre are responsible for the horizontal distribution of the electron cloud and for its dependence on the bunch population above the multipacting threshold.

The electron cloud surrounds the beam for N_{th}<N_b<0.5-0.6×10^{11}; above this population the electrons concentrate in two stripes, one on either side of the beam and parallel to the magnetic field lines (Fig. 18) and for N_b>1.1×10^{11} a third stripe centred on the beam appears [2,3,8].

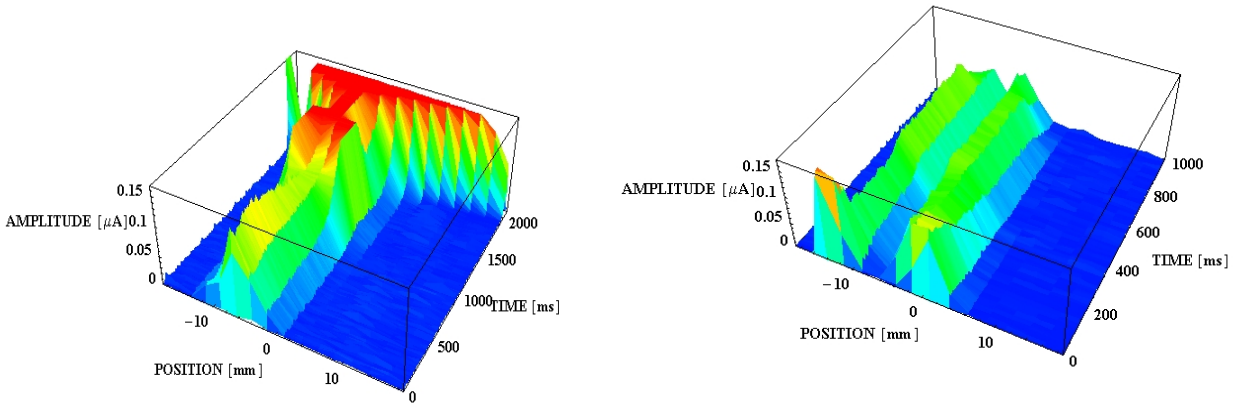

Figure 18. Horizontal distribution of the electrons vs. time in a dipole field region after injection of the LHC beam for N_b=0.5×10^{11} (left) and N_b=0.6×10^{11} (right). In the left plot the effect of the reduction of the magnetic field intensity (after 1000 ms) is visible. N_{th} was ~ 0.2-0.3×10^{11} during the measurement. The beam radial position was ~ -5 mm at the electron cloud monitor.

For low bunch populations (N_{th}<N_b<0.5-0.6×10^{11}) the electron cloud can be schematically approximated as a vertical ribbon of uniform charge density ρ_{ec} (Fig. 19) developing along the batch starting from a given bunch *n*.

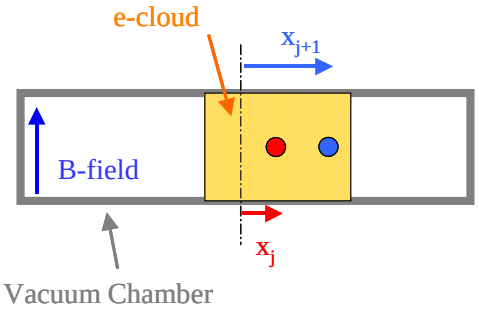

Figure 19. Schematic representation of the coupling of the motion of consecutive bunches due to the presence of the electron cloud.

When a bunch has a horizontal displacement with respect to the preceding one it will go through the electron cloud ribbon off-centre and will experience a linear force *F*:

$$F = -\frac{e\rho_{ec}}{\varepsilon_0}\left(x_{j+1} - x_j\right)\chi(j-n)$$

where x_j and x_{j+1} are the horizontal positions of bunch *j* and the following one, respectively and χ is the step function. In general the range of the coupling due to the electron cloud could be longer than the bunch spacing and one bunch could couple to more than one trailing bunch.

The behaviour of the 72 bunches can be described by the following set of coupled linear differential equations of the second order:

$$\frac{d^2x_l}{ds^2} + \left(\frac{Q}{R}\right)^2 x_l = -k_{ec}\sum_{k=1}^{72}\left(x_l - x_k e^{\frac{i(l-k)s_{bunch}}{R}Q}\right)\chi(k-n)F_{lk} \quad \text{with} \quad k_{ec} = \frac{1}{pc\beta}\frac{e\rho_{ec}}{\varepsilon_0}\frac{L_{arc}}{2\pi R} \tag{1}$$

where *s* is the longitudinal spatial coordinate along the machine, *R* is the machine radius, L_{arc} is the total length of the arcs, *Q* the unperturbed tune, s_{bunch} the bunch spacing, *p* the momentum of the beam and βc its speed, *e* is the electron charge magnitude, ε_0 is the permittivity of free space. The exponential term multiplying x_k takes into account the fact that the electron cloud seen by the bunch *l* is centred around the horizontal position occupied by the bunch *k*, $(l-k)s_{bunch}/\beta c$ seconds before. F_{lk} is a term describing the effective interaction length of the electron cloud wake and can be a simple rectangular function or an exponential function. In the case where consecutive bunches only are coupled and the phase term neglected, a degenerate system is obtained with two unstable eigen-frequencies [9]: *Q* and $Q+2k_{ec}R^2/2Q$. The second mode has a higher frequency, the corresponding tune shift is:

$$\Delta Q = \frac{1}{pc\beta}\frac{e\rho_{ec}}{4\pi\varepsilon_0}L_{arc}\langle\beta_H\rangle$$

where $<\beta_H>$ is the average horizontal Twiss function in the smooth accelerator model.

The tune shift depends linearly on the electron cloud density, it is inversely proportional to the momentum of the beam and it is not explicitly dependent on the bunch population. The bunch population affects the instability behaviour only via the density of the electron cloud distribution in the region traversed by the beam. The dependence of the growth rate of the instability on the bunch intensity is weak and the growth rate is the lowest for the intermediate bunch populations $0.5\times10^{11} < N_b < 1.1\times10^{11}$ when the electrons are concentrated in two separate stripes symmetric with respect to the beam.

The above model explains qualitatively the behaviour observed for the lower bunch population (N_b<0.5×10^{11}) when the electron cloud surrounds the beam and for small oscillation amplitudes it can be considered uniform. A better approximation to reality consists in solving the system (2) including the dipolar and quadrupolar components of the resistive wall wake (for a flat chamber) [10]:

$$\frac{d^2x_l}{ds^2} + \left(\frac{Q}{R}\right)^2 x_l = -k_{ec}\sum_{k=1}^{72}\left(x_l - x_k e^{\frac{i(l-k)s_{bunch}}{R}Q}\right)\chi(k-n)F_{lk} - \overbrace{k_{res}x_l}^{Quad.\ term} +$$

$$\overbrace{+k_{res}\sum_{k=1}^{72}\left[x_k e^{\frac{i(l-k)s_{bunch}}{R}Q}\left(\chi(l-k-1)\sum_{m=0}^{\infty}\frac{e^{i2\pi mQ}}{\sqrt{(l-k)s_{bunch}+m2\pi R}} + \chi(k-l)\sum_{m=1}^{\infty}\frac{e^{i2\pi mQ}}{\sqrt{(l-k)s_{bunch}+m2\pi R}}\right)\right]}^{Dipolar\ \ term} \tag{2}$$

$$\text{with} \quad k_{res} = \frac{N_b e^2}{p}\frac{F}{\pi b^3}\sqrt{\frac{Z_0\rho}{\pi\beta}}$$

Z_0 is the impedance of free space, F is a form factor ($=\pi^2/24$ for a flat chamber in the horizontal plane), b is the half-height of the vacuum chamber and ρ is the resistivity of the material of which the vacuum chamber is composed.

In that case for $N_b=0.3\times10^{11}$, assuming that the electron cloud has a charge density ρ_{ec} such that $\rho_{ec}/e = 1\times10^{12}$ m^{-3} and develops after 50 bunches, as observed experimentally, solving the system of differential equations we obtain that the most unstable modes have a growth rate of ~0.0254 turn^{-1} (i.e. ~40 turns) and a tune shift of +0.023, in good agreement with what measured experimentally (Fig. 20). In the model an exponential decay of the coupled-bunch electron cloud wake with a decay constant of 2 bunches (compatible with simulations of the coupled bunch electron cloud wake field [11]) has been assumed. The most unstable mode is mainly affecting the tail of the batch (Fig. 21).

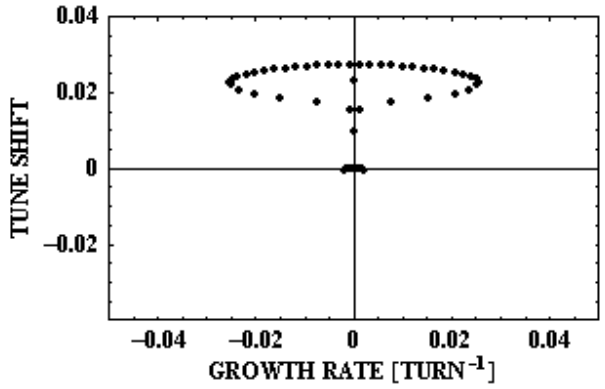

Figure 20. Tune shift and growth rates of the modes of the system of coupled oscillators described by Eqs. (1,2). The unstable modes have positive growth rates.

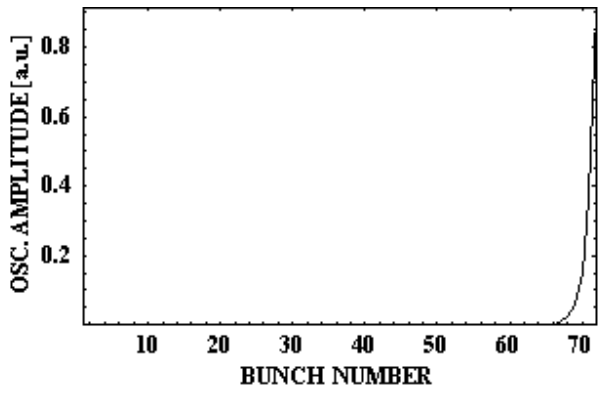

Figure 21. Amplitude of oscillation of the bunches in the most unstable mode. $N_b = 0.3\times10^{11}$, $\rho_{ec}/e=1\times10^{12}$ m^{-3}, it is assumed that the electron cloud develops after 50 bunches. The growth rate of this mode is ~0.0254 turn^{-1} (i.e. ~40 turns) and it has a tune shift of +0.023.

Vertical plane

In the vertical plane the motion of the electrons under the influence of the electric field of the bunch is not constrained by the presence of the magnetic field. The electron cloud is pinched during the bunch passage and the density of the cloud in the region traversed by the bunch is enhanced. The density evolution of the electron cloud with time depends on the bunch population. Any motion of the head of the bunch will couple to the tail as a wake field does. Because of the strong electron cloud density modulation during the bunch passage, differently from conventional wake fields, the electron cloud wake depends strongly on the position along the bunch from where it is excited and cannot be expressed simply in the form $W(z_s\text{-}z_w)$ where z_s and z_w are the longitudinal position of the source and witness particles, respectively. In general $W=W(z_s,z_w)$ is not invariant under translation. Because of this peculiarity of the electron cloud wake field the Transverse Mode Coupling Theory can be applied only as an approximation and an adequate formalism has to be developed [12].

ELECTRON CLOUD INSTABILITY IN THE PS WITH A MODIFIED LHC BEAM

Observations on the onset of the electron cloud instability have been performed also in the PS [13]. Here the LHC beam is normally extracted just after a non-adiabatic bunch length compression from 16 to 4 ns has taken place. Figure 22 shows the amplitude of the first unstable horizontal betatron line (1-q_H ~ 357 kHz) over 200 ms as measured with a spectrum analyser connected to a horizontal wide-band pick-up. In the first 55 ms two consecutive bunch splittings (from harmonics 21 to 84) take place. The bunch length is then kept equal to 16 ns for approximately 40 ms and it is finally adiabatically compressed to 10 ns in 5 ms (Fig. 22a). A horizontal instability develops for $N_b \geq 0.46\times10^{11}$ once the bunch length is shorter, the growth time τ is a few ms and it is not very sensitive to the bunch population, similarly to what has been observed in the SPS. For the higher bunch population ($N_b \geq 0.69\times10^{11}$) signs of the instability are observed already during the adiabatic bunch compression from 16 to 10 ns as indicated by the red circles in figures 22 c and d.

The measurements cannot exclude a coupled-bunch nature of the instability, although at higher order modes as compared to the SPS. No vertical instability has been detected but its growth rate could be longer than that for the horizontal instability at the intensities considered.

An emittance growth of a factor 10-20 and of a factor 2 in the horizontal and vertical planes, respectively, has been measured for the largest bunch population.

The above measurements have been conducted under conditions which are different from those for the production of the LHC beam in order to enhance the phenomenon and to study it in detail. Nevertheless at intensities higher than nominal electron cloud instabilities could occur also for the standard LHC beam production scheme in the PS.

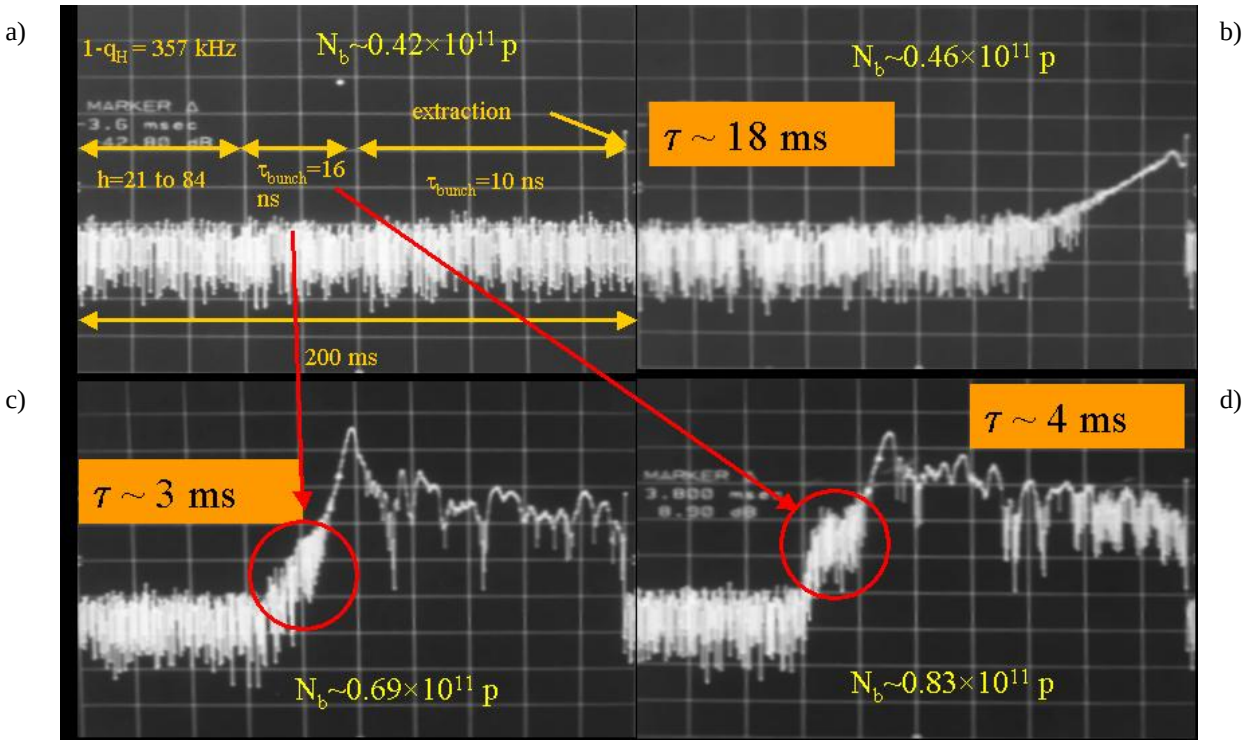

Figure 22. Amplitude of the first horizontal unstable line vs. time as measured by a spectrum analyser connected to a horizontal wide-band pick-up in the PS.

ELECTRON CLOUD EFFECTS WITH THE FIXED-TARGET BEAM IN THE SPS

In the SPS electron cloud effects have appeared not only in the presence of the LHC beam but also with the fixed target beam (see Table 2 for its main parameters) although only after a long shut-down, before conditioning with the LHC beam (scrubbing) [2,3].

Figure 23 shows the dynamic pressure increase measured with the fixed target beam as a function of its intensity, which has been increased step-by-step to identify the threshold for the onset of electron multipacting. The SPS supercycle is 16.8 s long and the fixed target beam remains in the machine for 9.12 s: during that time the fixed target beam is injected and accelerated to 400 GeV/c (in 4.32 s) and then slowly extracted with RF off. Multipacting occurs during acceleration and then disappears during extraction so that the vacuum pressure recovers before the next injection.

As for the LHC beam the threshold bunch population for the onset of electron multipacting is lower in the SPS arcs than in the straight sections. The corresponding values are listed in Table 3. Measurements of the electron cloud signal with dedicated monitors [8] show that electron multipacting is detected only during the ramp for momenta above 100 GeV/c.

Table 3. Threshold bunch population for the onset of electron multipacting in the SPS arcs, before conditioning with LHC beam.

Beam	N_{th} [10^{11}]
LHC-25ns (1 batch) - injection	0.2
Fixed-target (2 batches) -100 GeV/c	0.05

Figure 24 shows the electron cloud signal measured along the cycle. The peak-detected signal from a longitudinal pick-up is also shown. This is proportional to the inverse of the bunch length of the shortest bunch in the fixed target batch. Injection and transition are indicated. The latter corresponds to a maximum of the peak-detected signal but no electron-cloud signal is measured at transition. This seems to indicate that not only the bunch length is a critical parameter but that the transverse beam size might also play a role.

The correlation of the electron cloud signal with the bunch density, i.e. the quantity:

$$\frac{\text{Peak Detected Signal}}{\sigma_H \sigma_V} \qquad (3)$$

where σ_H and σ_V are the r.m.s. horizontal and vertical beam sizes measured along the cycle is not good, particularly during the last part of the ramp.

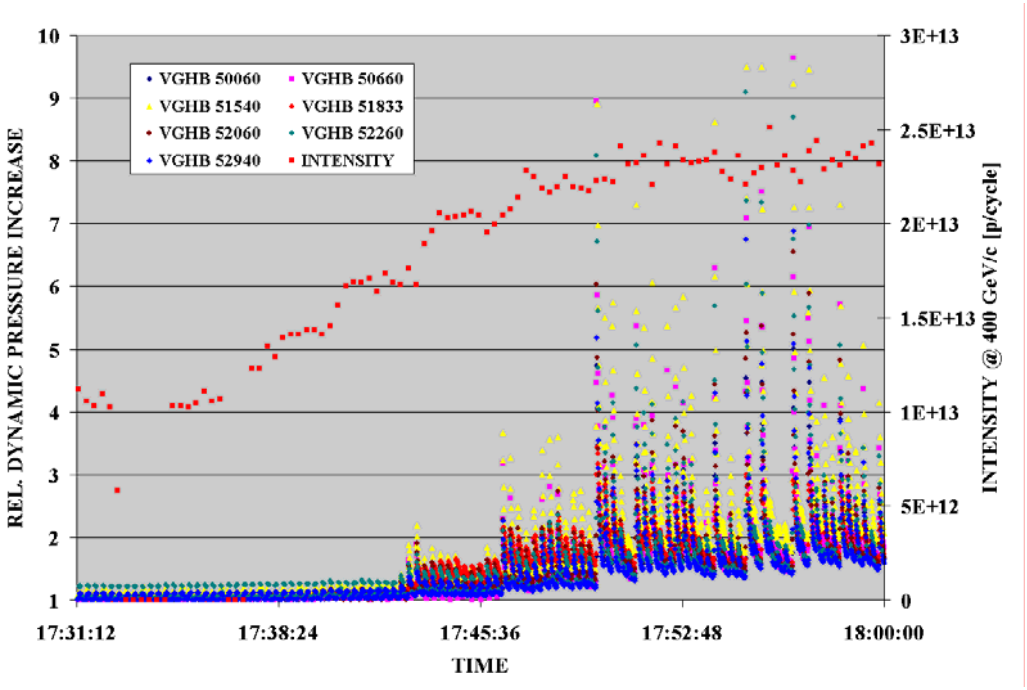

Figure 23. Dynamic pressure increase measured in the SPS with the fixed target beam. The total intensity has been increased in steps with time.

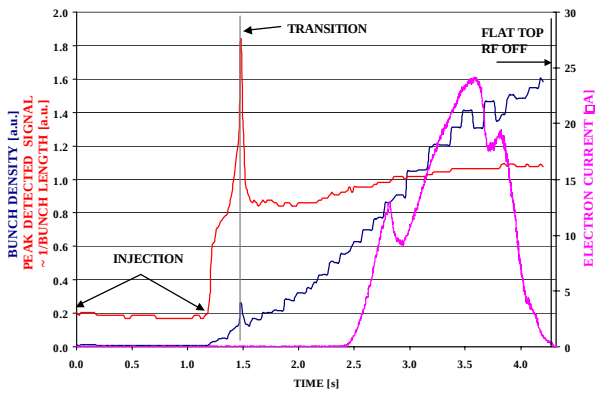

Figure 24. Electron cloud signal vs. time in the cycle. The peak detected signal from a longitudinal monitor and the "bunch density" are plotted as well.

A better correlation is obtained when the electron cloud signal is plotted versus the quantity:

$$\frac{1}{\sigma_t^4 \sigma_H \sigma_V} \qquad (4)$$

where σ_t is the average of the bunch length measured over 25 bunches of the fixed target beam (see Fig. 25). The reduction of the bunch length at transition is much less visible in these figure due to the coarser sampling of the bunch length measurement: a measurement of the longitudinal bunch profile was performed every 1200 turns (~28 ms).

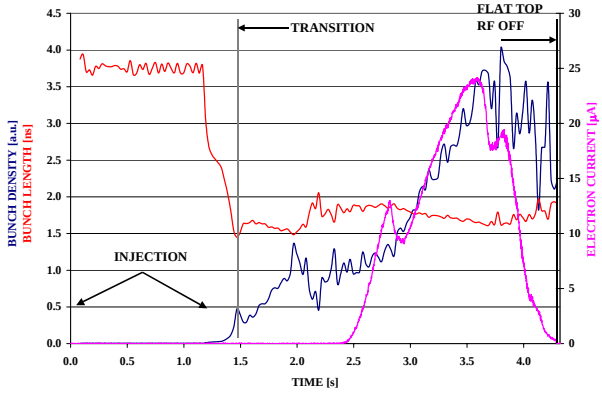

Figure 25. Electron cloud signal vs. time in the cycle. The average bunch length and the quantity in Eq. (4) are plotted vs. time as well.

OBSERVATIONS ON ELECTRON CLOUD LIFETIME IN THE SPS

In a standard SPS filling cycle for the LHC operation 2 to 4 consecutive PS bunch trains are injected with a spacing of 225 ns to allow enough space for the SPS injection kicker rise-time. In the LHC 12 of these SPS batches will be injected with a spacing of 975 or 1000 ns. Furthermore, while in the SPS only a fraction of the machine circumference (~1/3) is filled, in the LHC the filling factor is close to 1 [14]. The electron-cloud lifetime is therefore a critical parameter for its build-up with consecutive bunch trains and for its effect on beam stability. A short electron lifetime would imply in fact a

complete 'reset' of the electron cloud between batches and between consecutive turns.

Figure 26 shows the spectrum of the vertical motion of the centroids of the bunches of a LHC batch in which 12 consecutive bunches are missing (corresponding to a gap of 325 ns). In the leading part of the batch the instability develops only after approximately 20 bunches, in the trailing part of the batch following the beam gap the instability develops only after few bunches indicating that electrons have a survival time longer than 325 ns and can couple the bunch motion through the beam gap. The observation below is compatible with direct measurements of the electron flux vs. time for different spacings among LHC bunch trains [2,3]

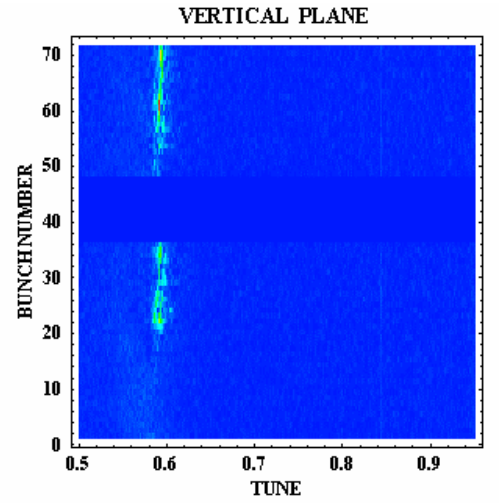

Figure 26. Density plots of the tune spectrum vs. bunch number in the vertical plane. N_b= 0.3×10^{11} > N_{th} ~ 0.2-0.3×10^{11}. The beam gap is localized between bunch number 37 and bunch 48 (included).

Other observations that could be relevant for the characterization of the electron cloud lifetime in the SPS have been collected during parallel operation of the LHC and fixed target beams on two consecutive cycles.

Figure 27 shows the SPS magnetic cycle for such type of operation. The fixed target beam circulates in the machine for the first 9.12 s while the LHC beam is injected 2.105 s after the slow extraction of the fixed target beam has been completed and circulates for 4.65 s. The fixed target beam is injected in the following super-cycle 925 ms after the dump of the LHC beam.

An enhancement of the electron cloud signal induced by the fixed target beam has been measured when an LHC beam is injected in the preceding cycle, even after conditioning of the SPS with LHC beams. This is shown in Fig. 28. Once the injection of the fixed target cycle is inhibited the above phenomenon disappears immediately in the following cycle.

The above observations could be explained either by a long lifetime of the electron cloud (e.g. by magnetic trapping in multipoles) [15,16] or as a consequence of the increase of the residual pressure resulting from the outgassing accompanying electron multipacting. The latter explanation is valid only if the electron cloud build-up during a single passage of the fixed target beam does not reach saturation, only in that case the electron cloud density will depend on the initial number of seed electrons and therefore on the residual pressure.

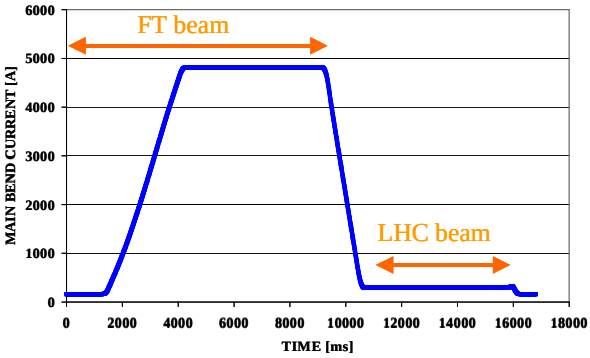

Figure 27. Standard SPS magnetic cycle for operation with fixed target and LHC beams in parallel.

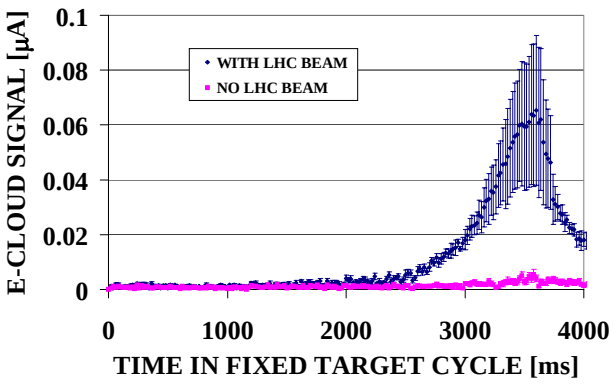

Figure 28. Enhancement of the electron cloud signal (in a region with magnetic field) on the fixed target cycle in the presence of LHC beam in the preceding cycle. The total intensity of the fixed target beam (2 batches) was 2.5×10^{13} p/cycle (corresponding to N_b~0.06×10^{11}) and the bunch population of the LHC beam (1 batch) was N_b=1.1×10^{11} > N_{th} ~ 0.8×10^{11}.

ELECTRON CLOUD INSTABILITY IN THE SPS WITH FIXED TARGET BEAM - OBSERVATIONS

FT beam in parallel to LHC beam operation

When the LHC beam is injected the fixed target beam in the cycle immediately following is affected by losses at injection energy. These are the consequence of a vertical instability affecting the tail of the fixed target batch. Inhibiting injection of the LHC beam eliminates this effect in the following fixed target cycle. Figure 29 shows the sum (Σ) and delta (Δy) signals form a vertical pick-up when no LHC beam is injected and when the LHC beam

is injected in the preceding cycle. The growth time of the instability is long (a few thousands turns) and it occurs even when the transverse feedback is active.

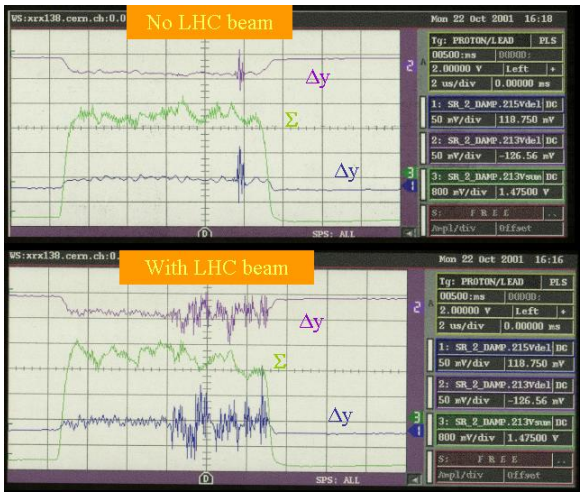

Figure 29. Sum (Σ) and delta (Δy) signals from two vertical pick-ups at injection energy, 500 ms after injection. The total intensity of the fixed target beam (1 batch) was 1.7×10^{13} p/cycle (corresponding to N_b~0.08×10^{11}).

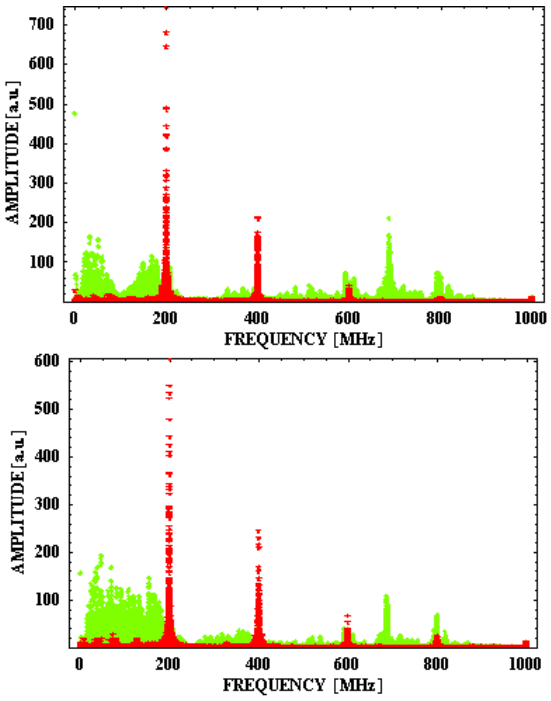

Figure 30. Fourier spectra of the sum (red) and delta (green) signals from a wideband vertical pick-up for the fixed target beam (1 batch - ~1.4×10^{13} p/cycle - N_b~0.07×10^{11}) 100 ms after injection. The transverse feedback was ON during the measurements. The top and bottom plots refer to data taken in similar conditions.

High order coupled-bunch modes (max. 50 MHz but sometimes up to the highest – 100 MHz) are visible in the vertical plane and the transverse feedback can damp only modes up to ~20 MHz. Single-bunch modes at about 700MHz are also distinguishable (Figure 30). Coupled-bunch instabilities up to the highest modes develop very likely because of the lower bunch charge and tighter bunch spacing resulting in a electron bouncing period longer than the bunch spacing. Measured rise times are much longer than those observed for the nominal LHC beam.

In the horizontal plane, only low order coupled bunch modes (<10 MHz) can occur because the electron cloud motion is frozen in that plane during the bunch passage. These modes are damped by the transverse feedback.

Dedicated operation with fixed-target beam

For the conditions explored up to now (N_b<0.1×10^{11}) the electron cloud instability is not a serious problem for the fixed-target beam in the SPS because the electron cloud build-up occurs mainly at high energy when the beam is stiffer, even before conditioning with the LHC beam.

Nevertheless other undesirable electron cloud effects have been noticed, in particular sparking of the electrostatic septa.

CURES FOR THE ELECTRON CLOUD INSTABILITY

Horizontal plane

In the SPS the coupled-bunch instabilities excited in this plane have low-order modes and can be cured by means of the transverse feedback [17]. In the PS, where a transverse feedback is not available, octupoles proved to have a marginal effect on the observed electron cloud instability whose nature (single or coupled bunch) needs to be studied in more detail. Nevertheless it must be noted that the available strength of these elements is limited and the induced tune spread at half-width-half-height is limited to few 10^{-5} [13].

Vertical plane

Single bunch instabilities, like those observed on LHC beam in the SPS, can be cured with high chromaticity $\xi = (\Delta Q/Q)/(\Delta p/p) \sim 0.5–1$ [17].

Coupled-bunch instabilities, like those arising on the fixed-target beam during parallel operation with the LHC beam in the SPS, can be cured with octupoles.

Other solutions

The increase of the threshold for the onset of the electron cloud build-up is of course the preferred method to reduce the electron cloud density and therefore to fight electron cloud instabilities. A reduction of the Secondary Emission Yield is instrumental in increasing the threshold for electron multipacting and can be achieved by electron bombardment induced by the beam (“beam scrubbing”)

[2,3]. This method has been successfully applied in the SPS. Although a complete suppression of electron multipacting in the arcs cannot be obtained (the threshold for the onset of the beam-induced electron multipacting is N_{th}=0.8×10^{11} after scrubbing) a significant attenuation of the electron cloud effects has been observed, as shown in Fig. 31. A clear reduction of the vertical emittance growth of the LHC beam has been observed during the scrubbing run although the beam intensity has been increased and the vertical chromaticity (applied to cure the vertical electron cloud instability) has been reduced with time (down to $\xi \sim 0.2$).

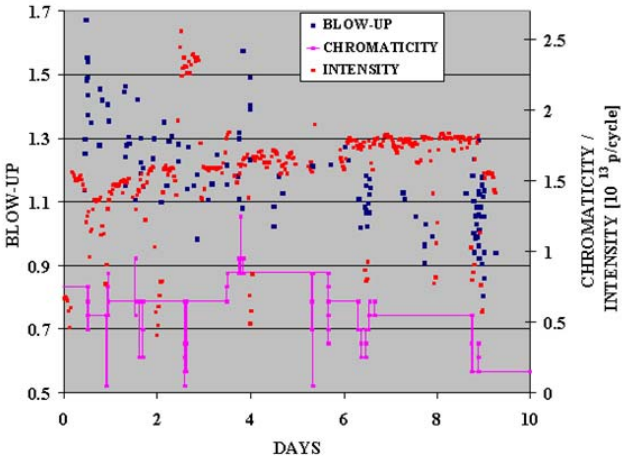

Figure 31. Measured vertical LHC beam emittance growth (blue) along a 15 s injection plateau during the SPS scrubbing run in 2002. The total intensity of the beam (red) and the vertical chromaticity settings (purple) are plotted as well.

SUMMARY AND CONCLUSIONS

Electron cloud effects have been observed in the PS Complex and SPS, initially with LHC beams

Fast instabilities are the most dramatic effect on the beam. Their nature is the result of the behaviour of the electron cloud in the bending magnets, filling a large fraction of the circumference of these machines.

Electron cloud build-up has been observed in the SPS also for the fixed target beam, but for the intensities accelerated so far, only at high energy and in a machine that has not been conditioned with LHC beam. Electron cloud effects have been noticed at injection only when the SPS has been operated with fixed-target and LHC beams in parallel.

The electron-cloud lifetime is larger or comparable to the beam gap between consecutive PS LHC bunch trains injected in the SPS or consecutive SPS LHC bunch trains injected in the LHC. Preliminary indications of even longer electron survival have been collected and need further investigations.

Cures have been developed to reduce electron multipacting and to control the electron cloud instability in the SPS, as a result of which LHC beams with nominal bunch population and longitudinal emittance and with transverse emittances close to nominal ($\varepsilon^*_H = \varepsilon^*_{nominal}$ and $\varepsilon^*_V \sim 1.2\ \varepsilon^*_{nominal}$) have been accelerated up to the SPS extraction energy in 2003 [18].

ACKNOWLEDGEMENTS

We would like to thank the colleagues of the AB/OP and AB/RF groups for the contribution to the setting-up of the beams used during the studies.

REFERENCES

[1] P. Collier Ed., “The SPS as Injector for LHC – Conceptual Design”, CERN/SL/97-07 DI.

[2] J.-M. Jimenez et al., “Electron Cloud Studies and Analyses at SPS for LHC-Type Beams”, Proceedings of the 2003 Particle Accelerator Conference, Portland, Oregon, USA, May 12-16, 2003, J. Chew, P. Lucas, and S. Webber, Eds, p. 307-311.

[3] J. M. Jimenez et al., “Electron Clouds, Results from SPS and Experiments for 2003”, Proceedings of the Workshop on LHC Performance - Chamonix XII, 3-8 March 2003, Chamonix (France), J. Poole, S. Dubourg and M. Truchet Eds., CERN AB/2003-008 ADM, p. 327-334.

[4] W. Höfle, “Observation of the Electron Cloud Effect on Pick-up Signals in the SPS”, Proceedings of the Workshop on LEP-SPS Performance - Chamonix X, 17-21 January 2000, Chamonix (France), P. Le Roux, J. Poole, M. Truchet Eds., CERN SL/2000-007(DI), p. 112-118.

[5] K. Cornelis, “The Electron Cloud Instability in the SPS”, Mini-Workshop on Electron Cloud Simulations for Proton and Positron Beams - ECLOUD'02, 15 - 18 April 2002, CERN, Geneva, Switzerland, CERN-2002-001, G. Rumolo and F. Zimmermann Eds., p. 11-16.

[6] R. Jones, “Progress with Beam Instrumentation”, Proceedings of the LHC Workshop - Chamonix XI, 15-19 January 2001, Chamonix (France), J. Poole Ed., CERN SL/2001-003(DI), p. 101-107.

[7] Y. Ohnishi et al., “Study of the Fast Ion Instability at KEKB Electron Ring”, Proceedings of the 7th European Particle Accelerator Conference (EPAC2000), 26-30 June 2000, Vienna (Austria), p. 1167-1169.

[8] G. Arduini et al., “Measurement of the Electron Cloud Properties by means of a Multi-Strip Detector in the CERN SPS”, CERN SL-2002-055-OP. Proceedings of the 2002 European Particle Accelerator Conference, 3-7 June 2002, Paris, France, T. Garvey, J. Le Duff, P. Le Roux, Ch. Petit-Jean-Genaz, J. Poole, L. Rivkin, Eds., p. 1437-1439.

[9] K. Cornelis, “The Electron cloud Instability in the SPS”, Mini-Workshop on Electron Cloud Simulations for Proton and Positron Beams - ECLOUD'02, 15 - 18 April 2002, CERN, Geneva, Switzerland, CERN-2002-001, G. Rumolo and F. Zimmermann Eds., pp. 11-16.

[10] J. Gareyte, “Impedances: Measurements and Calculations for Non-symmetric Structures” Proceedings of the 2002 European Particle Accelerator Conference, 3-7 June 2002, Paris, France, T. Garvey, J. Le Duff, P. Le Roux, Ch. Petit-Jean-Genaz, J. Poole, L. Rivkin, Eds., p. 89-93 and references therein

[11] D. Schulte, private communication (2003).

[12] E. Perevedentsev, “Head-Tail Instability Caused by Electron Cloud”, Mini-Workshop on Electron Cloud Simulations for Proton and Positron Beams - ECLOUD'02, 15 - 18 April 2002, CERN, Geneva, Switzerland, CERN-

2002-001, G. Rumolo and F. Zimmermann Eds., pp. 171-194.

[13] R. Cappi et al., “Electron cloud build-up and related instability in the CERN Proton Synchrotron”, PRST-AB, 5, 094401 (2002).

[14] P. Collier, “Baseline Proton Filling Schemes”, Proceedings of the LHC Project Workshop – Chamonix XIII – 19-23 January 2004, Chamonix (France), J. Poole, T. Kehrer and M. Truchet Eds., CERN AB/2004-014 ADM, p. 30-33.

[15] G. Rumolo, F. Zimmermann, “Electron Cloud Simulations: Build-up and Related Effects”, Mini-Workshop on Electron Cloud Simulations for Proton and Positron Beams - ECLOUD'02, 15 - 18 April 2002, CERN, Geneva, Switzerland, CERN-2002-001, G. Rumolo and F. Zimmermann Eds., p. 97-111.

[16] L. F. Wang at al.,”3D Simulation of Photoelectron Cloud in KEKB LER”, Mini-Workshop on Electron Cloud Simulations for Proton and Positron Beams - ECLOUD'02, 15 - 18 April 2002, CERN, Geneva, Switzerland, CERN-2002-001, G. Rumolo and F. Zimmermann Eds., p. 113-121.

[17] G. Arduini, K. Cornelis, W. Höfle, G. Rumolo, F. Zimmermann, “The Electron Cloud Instability of the LHC Beam in the CERN SPS”. CERN-LHC-Project-Report-637. Proceedings of the 2003 Particle Accelerator Conference, Portland, Oregon, USA, May 12-16, 2003, J. Chew, P. Lucas, and S. Webber, Eds, p. 3038-3040.

[18] G. Arduini, “LHC Beams in the SPS: Where Do We Stand?”, Proceedings of the LHC Project Workshop – Chamonix XIII – 19-23 January 2004, Chamonix (France), J. Poole, T. Kehrer and M. Truchet Eds., CERN AB/2004-014 ADM, p. 34-43.